

## Computer simulations of stimulus dependent state switching in basic circuits of bursting neurons

Mikhail Rabinovich,<sup>1</sup> Ramón Huerta,<sup>1,2</sup> Maxim Bazhenov,<sup>3</sup> Alexander K. Kozlov,<sup>4</sup> and Henry D. I. Abarbanel<sup>5,\*</sup>

<sup>1</sup>*Institute for Nonlinear Science, University of California, San Diego, La Jolla, California 92093-0402*

<sup>2</sup>*Department of Computer Engineering, Universidad Autónoma de Madrid, 29049 Madrid, Spain*

<sup>3</sup>*Howard Hughes Medical Institute, The Salk Institute, Computational Neurobiology Laboratory, La Jolla, California 92037*

<sup>4</sup>*Institute of Applied Physics, Russian Academy of Sciences, 46 Ulyanov Street, Nizhny Novgorod 603600, Russia*

<sup>5</sup>*Department of Physics and Marine Physical Laboratory, Scripps Institution of Oceanography, University of California, San Diego, Mail Code 0402, La Jolla, California 92093-0402*

(Received 27 January 1998; revised manuscript received 23 July 1998)

We investigate the ability of oscillating neural circuits to switch between different states of oscillation in two basic neural circuits. We model two quite distinct small neural circuits. The first circuit is based on invertebrate central pattern generator (CPG) studies [A. I. Selverston and M. Moulins, *The Crustacean Stomatogastric System* (Springer-Verlag, Berlin, 1987)] and is composed of two neurons coupled via both gap junction and inhibitory synapses. The second consists of coupled pairs of interconnected thalamocortical relay and thalamic reticular neurons with both inhibitory and excitatory synaptic coupling. The latter is an elementary unit of the thalamic networks passing sensory information to the cerebral cortex [M. Steriade, D. A. McCormick, and T. J. Sejnowski, *Science* **262**, 679 (1993)]. Both circuits have contradictory coupling between symmetric parts. The thalamocortical model has excitatory and inhibitory connections and the CPG has reciprocal inhibitory and electrical coupling. We describe the dynamics of the individual neurons in these circuits by conductance based ordinary differential equations of Hodgkin-Huxley type [J. Physiol. (London) **117**, 500 (1952)]. Both model circuits exhibit bistability and hysteresis in a wide region of coupling strengths. The two main modes of behavior are in-phase and out-of-phase oscillations of the symmetric parts of the network. We investigate the response of these circuits, while they are operating in bistable regimes, to externally imposed excitatory spike trains with varying interspike timing and small amplitude pulses. These are meant to represent spike trains received by the basic circuits from sensory neurons. Circuits operating in a bistable region are sensitive to the frequency of these excitatory inputs. Frequency variations lead to changes from in-phase to out-of-phase coordination or vice versa. The signaling information contained in a spike train driving the network can place the circuit into one or another state depending on the interspike interval and this happens within a few spikes. These states are maintained by the basic circuit after the input signal is ended. When a new signal of the correct frequency enters the circuit, it can be switched to another state with the same ease. [S1063-651X(98)13011-8]

PACS number(s): 87.10.+e, 87.22.As

### I. INTRODUCTION

Many experiments indicate that spiking-bursting neurons have special importance for rhythmic motor control [1,3,4] and oscillatory brain functions [5,6]. In neural assemblies the collective dynamics of such neurons may generate a set of characteristic phase differences or time lags that represent distinct states of the oscillatory behavior. Oscillatory circuits with quite different architectures may show similar dynamical features and we inquire here into a potential utilization of the similarities of such diverse neural circuits. We investigate two basic neural circuits, which are presented in Fig. 1. Figure 1(a) shows a neural couple from the lobster stomatogastric ganglion (STG) [1] and Fig. 1(b) a typical vertebrate thalamocortical circuit [2]. Although the functional role played by these circuits is very different, the presence of antagonistic coupling between different parts of the circuit makes them exhibit common dynamical features. In the central pattern generator (CPG) circuit the antagonistic coupling

is given by the electrical and inhibitory connections. The electrical coupling tends to drive the two neurons into closely in-phase synchronized oscillations, while the inhibitory couplings lead to a tendency for out-of-phase oscillations. In the thalamocortical circuit the two sides of the assembly are connected by both excitatory and inhibitory links.

In this paper we inquire into the utility of such antagonistic connections in neural circuitry. In a general way we expect excitatory neural connections and electrical connections to produce in-phase bursting oscillations, while mutual inhibitory coupling tends to produce out-of-phase behavior for the coupled neurons. The exceptions to this “rule” are discussed in [7–9]. In particular, in [10] it was shown that if the rise time of the synapse is longer than the duration of an action potential, inhibition not excitation leads to synchronized firing. We suggest here, following earlier work [11], that this antagonistic structure of neural connections can be important for organizing bistable or multistable behavior in neural circuits. We should note that a multistability may appear in the coupled spiking-bursting neurons connected with a gap junction [12] or synaptic exponential coupling [10] alone; however, the region of multistability is usually broader in systems with contradictory coupling. Such multistability can facilitate the storage and encoding of informa-

\*Present address: Institute for Nonlinear Science, University of California–San Diego, La Jolla, CA 92093-0402. FAX: 619-534-7664. Electronic address: hdia@hamilton.ucsd.edu

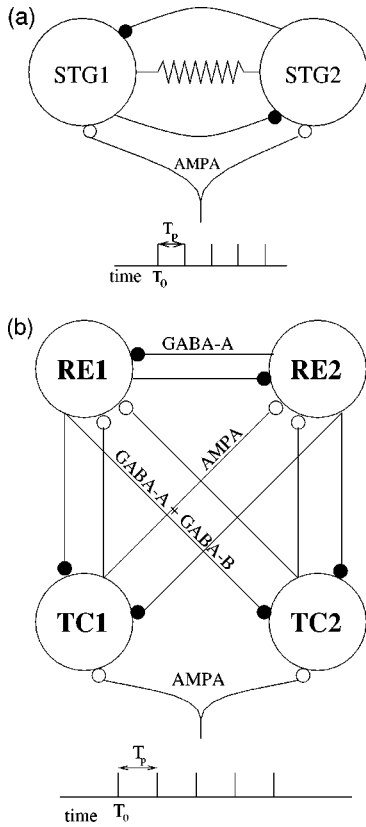


FIG. 1. Basic circuits: (a) CPG circuit and (b) thalamocortical circuit. Solid circles indicate inhibitory connections and open circles excitatory connections. The resistor symbol denotes a gap junction connection. The manner in which the external inputs were introduced through AMPA excitatory synapses is also shown. Shown beneath each circuit is a schematic representation of the input spike trains. The input signals started at a time  $T_0$  and were spaced by  $T_p$ . We investigated the dependence of attractor switching on the spike timing  $T_p$ . A sample of the responses of the basic circuits to inputs with different  $T_p$  can be seen in Figs. 4 and 9. Also in those figures is a more realistic picture of the incoming spike trains.

tion that is received by neural assemblies. We will show here that the switching of the circuit from one state to another can be accomplished by an incoming spike train and that whether the switch is made depends on the frequency of the spike train. After the spike train is completed, the circuit remains in the state where the spike impulses left it until another spike train of appropriate frequency comes along to switch it.

We begin by analyzing the autonomous bursting activity of these circuits using conductance based models of each neural element embodied in Hodgkin-Huxley differential equations. A common feature of oscillations in these circuits is a broad region of bistability encountered as interneural coupling strengths are varied. In many regions of parameter space at least two stable attractors coexist in the dynamical state space [13]. One attractor is associated with in-phase oscillations of the parts of the circuit and the other one is associated with out-of-phase oscillations. We then inject excitatory input, made up of short intervals of periodic spike trains, into the circuit as shown in Fig. 1. We find broad stable regions of spike train frequency where the input switches the circuit between the two main modes of oscillation.

## II. MODELS

We describe the behavior of an individual neuron by a system of ordinary differential equations of Hodgkin-Huxley type [14]. Such conductance-based models of neural dynamics provide a realistic description for the generation of action potential spikes as well as of the bursting behavior. The detailed equations for the membrane potential and the other dynamical quantities are described in the Appendix. The synaptic couplings are represented by kinetic models consistent with the Hodgkin-Huxley formalism in modeling ionic channels. Our model systems have been integrated using several independent methods: embedded Runge-Kutta 6(5) [15], backward differentiation [16], and in some cases implicit Runge-Kutta [17] methods. The results from each of the different methods of numerical integration were consistent with each other.

### A. CPG system

The autonomous dynamics of the model stomatogastric neuron is qualitatively as follows. There is a slow inward, depolarizing current  $I_h$  that drives the membrane potential to the point where a fast calcium current  $I_{Ca}$  is activated. This is the beginning of the burst. The  $I_{Ca}$  leads to the activation of  $I_{Na}$ , which depolarizes the cell and generates action potentials or spikes. While  $I_{Ca}$  is activated, the calcium concentration inside the cell is raised. It produces activation of the potassium current  $I_K(Ca)$ , which determines the end of the burst. The cycle is repeated with the reactivation of  $I_h$ . In this circuit each neuron has intrinsic oscillations. When coupled by inhibitory and electrical synapses as shown in Fig. 1(a), the pair of STG neurons produced bursts that were either in phase or out of phase. Over a range of the electrical coupling  $g_{ele}$ ,  $5 \text{ nS} \leq g_{ele} \leq 12 \text{ nS}$ , more than one attractor was present in the state space of the CPG circuit.

In Fig. 2(c) we show the time lag between the right and left neural oscillators in this circuit as a function of the gap junction or electrical coupling  $g_{ele}$  between them. The inhibitory couplings were held fixed at  $g_{syn} = 20 \text{ nS}$ . This is the value we use for all the calculations reported here. When the time lag between the neurons is zero, we have in-phase behavior. As we increase  $g_{ele}$  from zero, the oscillations are out of phase with a time lag about 90 ms [Fig. 2(b)]. This time lag varies little until  $g_{ele} \approx 12 \text{ nS}$ . At that point the time lag drops rapidly to zero and the system oscillates in phase [Fig. 2(a)]. As we turn the value of  $g_{ele}$  down from  $g_{ele} > 15 \text{ nS}$ , the in-phase oscillations persist until  $g_{ele} \approx 5 \text{ nS}$  and then the system returns to out-of-phase behavior again. This difference in the state of the system as we reach certain values of  $g_{ele}$  from above or from below is the hysteresis or bistability we noted earlier. In Fig. 2(c) we also have cases where a small amount of Gaussian noise was added to each ionic conductance  $g_i$ . We represented this noise by

$$g_i(\epsilon) = g_i + \epsilon\sigma(t),$$

where  $\sigma(t)$  is white noise  $\langle\sigma(t)\rangle = 0$  and  $\langle\sigma(t)\sigma(t')\rangle = \delta(t - t')$ . We studied two cases:  $\epsilon = 0.1 \text{ nS}$  and  $\epsilon = 1.0 \text{ nS}$ . One can see that the hysteresis is quite robust against environmental noise affecting the synaptic conductances. Indeed, it was a surprise to us that the smaller noise level  $\epsilon = 0.1$  actu-

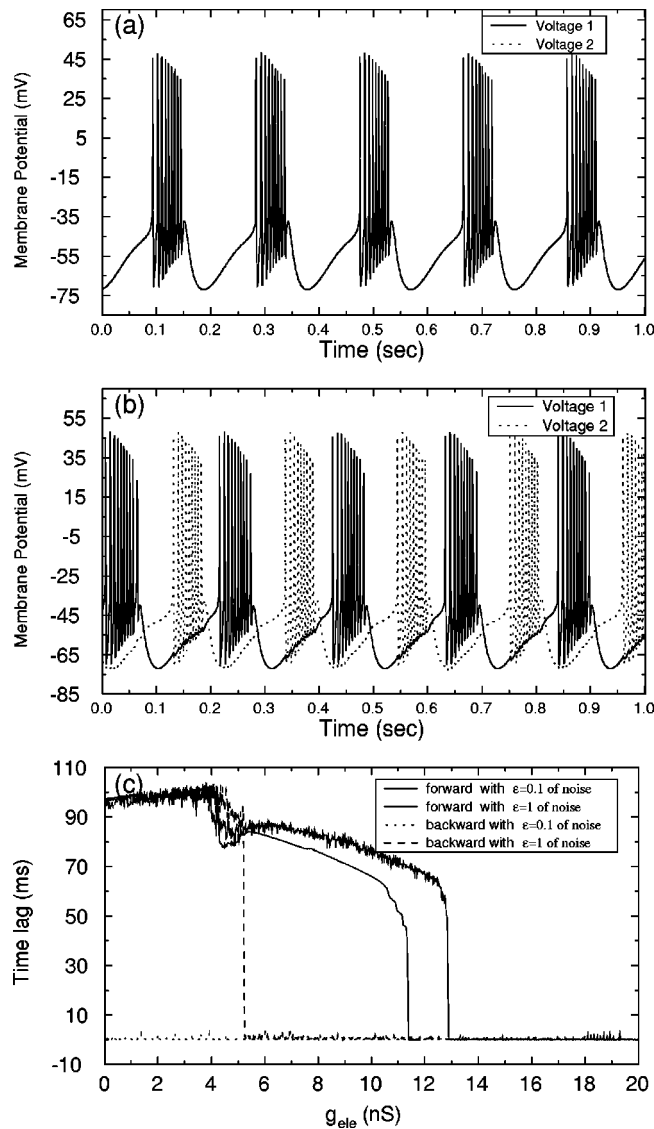


FIG. 2. Autonomous dynamics of the basic circuits showing the bistability that is critical to our investigations in this paper. (a) In-phase oscillations of the CPG neurons when  $g_{ele}=4$  nS and  $g_{syn}=20$  nS. (b) Out-of-phase oscillations of the CPG neurons when  $g_{ele}=4$  nS and  $g_{syn}=20$  nS. (c) Time lag between the oscillations of the CPG cells as a function of  $g_{ele}$  when  $g_{syn}=20$  nS. Here “forward” means that the control parameter  $g_{ele}$  is increased very slowly and “backward” means that  $g_{ele}$  is reduced very slowly. We also show the effect of small amounts of Gaussian white noise added to the conductances on the bistability or hysteresis in this CPG circuit. In the calculations we took each circuit conductance to have the form  $g(\epsilon)=g+\epsilon\sigma(t)$  with  $\sigma(t)$  Gaussian white noise with a rms value of unity. Cases with  $\epsilon=0.1$  nS and  $\epsilon=1.0$  nS are shown.

ally expanded the region of bistability where stable in-phase and out-of-phase oscillations both appear at the same system parameter values. Looking at this effect from the point of view of the neurons as a dynamical system, this suggests a shallow basin boundary between the two states at some values of  $g_{ele}$ . The robustness of these phenomena means that the switching between system attractors we shall report on shortly is a good candidate for a reliable biological mechanism.

## B. Thalamocortical system

Thalamic relay cells exhibit two different modes of behavior: the relay mode and burst mode. In the relay mode, corresponding to the awake state, thalamocortical (TC) cells are depolarized above  $-60$  mV. External sensory input evokes a train of action potentials transmitting sensory input to the cortex. Hyperpolarization of thalamic relay cells during sleep makes possible a deinactivation of low-threshold  $Ca^{2+}$  currents and leads to the burst mode. In this case the thalamus generates specific sleep-related oscillations and thalamic relay cells no longer relay sensory input to the cortex. In contrast, synchronization of thalamic oscillations by specific sensory signals will evoke a powerful input to the cortex.

Sleeping thalamic oscillations are generated as a result of synaptic interaction between thalamic relay cells and neurons of the thalamic reticular nucleus [2]. The lateral inhibitory  $\gamma$ -aminobutyric acid-A ( $GABA_A$ ) mediated connections between reticular (RE) neurons form a network that plays an important role in the generation and spreading of thalamic oscillations. TC cells receive a large  $GABA$ ergic input from RE cells and send back an excitatory  $\alpha$ -amino-3-hydroxy-5-methyl-4-isoxazolepropionic acid (AMPA) connection. The simplest network taking into account the essential features of thalamic organization and generating specific thalamic rhythms consists of pairs of coupled RE and TC cells and is shown in Fig. 1(b).

A detailed description of the dynamics of the TC and RE cells is contained in the Appendix. Here we give a qualitative discussion of the behavior of these cells.

The isolated TC cell shows self-sustained, slow  $\delta$  oscillations due to the interaction between the low-threshold  $Ca^{2+}$  current  $I_T$  and the hyperpolarization-activated cation current  $I_h$  [18,19]. Depolarization of the TC cell during burst discharge deactivates the  $I_h$  current resulting in a hyperpolarization of the cell. Hyperpolarization of the membrane potential leads to deinactivation of the low-threshold  $I_T$  current and activation of the  $I_h$  current, which slowly depolarizes the cell until it generates a new low-threshold spike. The RE cell has no intrinsic mechanisms for self-oscillations for the currents considered in the model. However, two RE cells coupled by inhibition can oscillate as a result of an interaction between low-threshold  $Ca^{2+}$  currents and  $GABA_A$  inhibitory postsynaptic currents [20,21].

The dynamics of the circuit seen in Fig. 1(b) arises from the interplay of cellular and synaptic properties in the TC and RE cells. The bursts in the RE cells activate  $GABA_A$  and  $GABA_B$  receptors in the TC cells and this results in their hyperpolarization followed by deinactivation of the  $I_T$  current and low-threshold spikes (LTSS). Burst discharges in the TC cells evoke excitatory postsynaptic potentials (EPSPs) in RE cells followed by the activation of the  $I_T$  current. Weak reciprocal inhibition between the RE cells produces prolonged burst discharges that activate  $GABA_B$  receptors in TC cells and synchronize them in phase as seen in Fig. 3(a). However, strong reciprocal inhibitory coupling between RE cells depresses burst discharges in these cells and the TC cells exhibit an out-of-phase rhythm shown in Fig. 3(b). This is typical for spindle oscillations [22,23]. Figure 3(c) gives the time lag between TC cells as a function of maximal

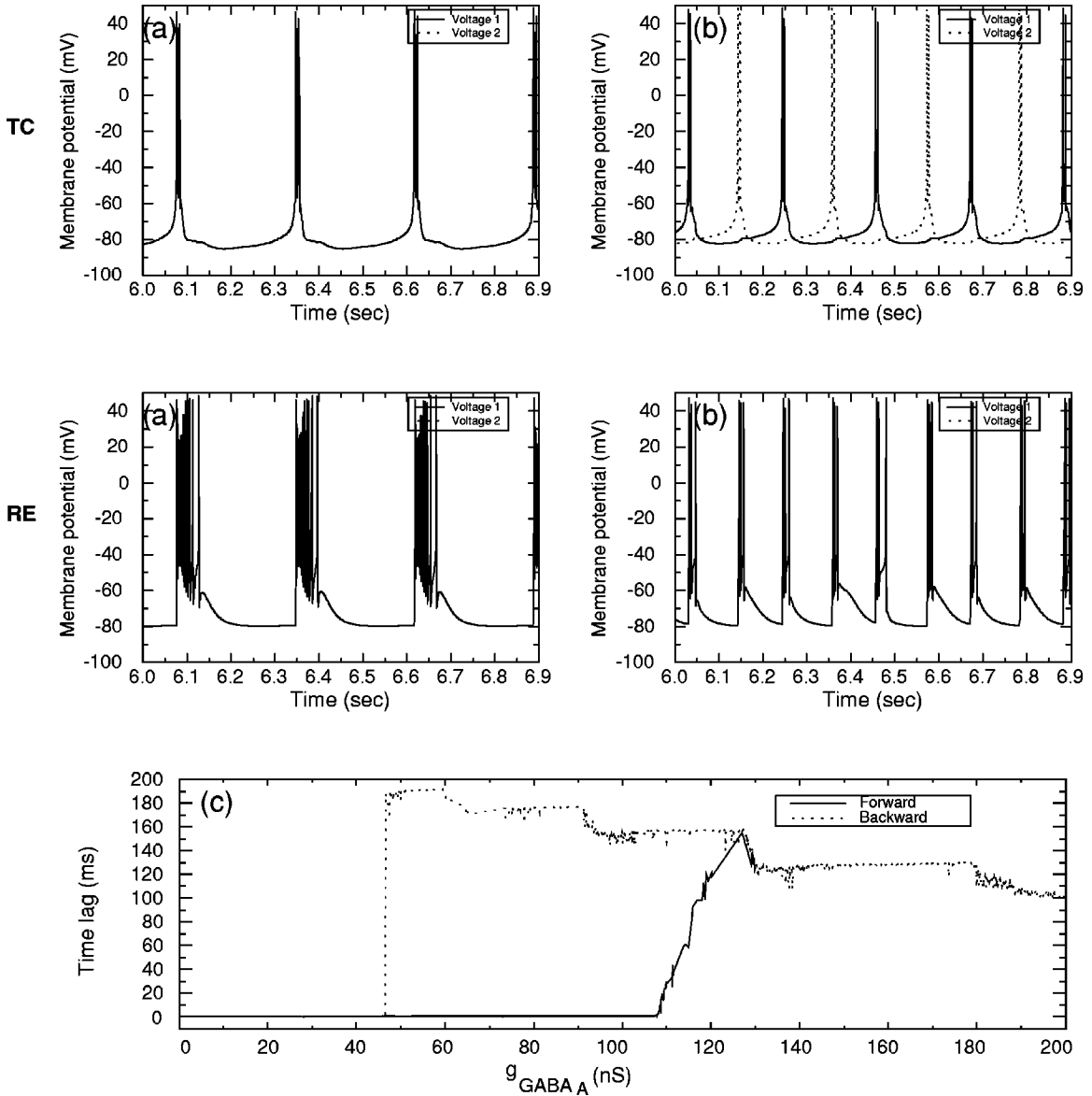


FIG. 3. Autonomous dynamics of the basic RE-TC circuit. (a) In-phase oscillations. Both RE and TC cells oscillate synchronously at  $\sim 3$  Hz. (b) Out-of-phase oscillations. RE cells oscillate synchronously at  $\sim 10$  Hz while TC cells produce bursts each second cycle with a frequency  $\sim 5$  Hz. (c) Time lag between the oscillations in TC cells as a function of  $g_{\text{GABA}_A}$  between RE cells. “Forward” means that the control parameter  $g_{\text{GABA}_A}$  is increased very slowly. “Backward” means that  $g_{\text{GABA}_A}$  is reduced very slowly.

$\text{GABA}_A$  conductance between RE cells. We can see a large region of bistability  $44 \text{ nS} \leq g_{\text{GABA}_A} \leq 110 \text{ nS}$  where the system exhibits in-phase or out-of-phase behavior depending on the initial conditions.

### III. FREQUENCY DEPENDENCE OF STATE SWITCHING

With the dynamical behavior of each circuit established, we now turn to the response of these basic neural assemblies to stimulation by a series of depolarizing spikes of varying interspike interval. The external forcing associated with these spike trains is mediated by AMPA receptors as shown in Fig. 1.

At the synaptic junctions, neurotransmitter is released at times

$$t_n = nT_p + T_0, \quad n = 1, 2, \dots, N_s,$$

where  $n$  is the spike number in a spike train consisting of  $N_s$  spikes.  $T_p$  is the time between spikes. The spike train starts at  $T_0$ . The release of this neurotransmitter initiates the spike train by driving the fraction of open channels  $[O](t)$  from zero to a value determined by the simple kinematics below.  $[O](t)$  itself enters the description of the AMPA current as

$$I_{\text{AMPA}}(t) = g_{\text{AMPA}}[O](t)\{V(t) - E_{\text{AMPA}}\},$$

and this is added to the dynamical equations of each neuron directly receiving external output. In our calculations we used  $g_{\text{AMPA}} = 50 \text{ nS}$  and  $E_{\text{AMPA}} = 0$ .

The simplified dynamics of  $[O](t)$  was taken to be

$$\frac{d[O](t)}{dt} = \alpha\{1 - [O](t)\}[T](t) - \beta[O](t),$$

where the timing information on the spikes is in the neurotransmitter concentration represented by

$$[T](t) = A \sum_{n=1}^{N_s} \theta(t_{\max} - t_n) \theta(t_n).$$

$A$  is the overall amplitude of neurotransmitter.  $A$ ,  $\alpha$ ,  $\beta$ , and  $t_{\max}$  are constants given in the Appendix.  $\theta(\cdot)$  is the Heaviside function.  $N_s$  spikes initiated at times  $t_n$  with spacing  $T_p$  are delivered to the circuit. We start a spike train by selecting a series of  $T_0$  and then associating that with a  $T_p$  and a number of spikes. The latter is chosen so that the spike train lasts about 1 s. Figures 4 and 9 show examples of how we can initiate spike trains at various  $T_0$  and have them inject current into the AMPA connections at interspike intervals of  $T_p$ . We vary  $T_p$  to investigate the dependence of the circuit response to the interpulse interval, stimulus length, and amplitude.

In each basic circuit, we explore the dependence on  $T_p$  of in-phase or out-of-phase synchronization of the parts of the circuit. We also examine the persistence of changes in the oscillations after the  $N_s$  spikes have passed.

We made the external AMPA synaptic connections slightly unsymmetric to provide both some realism in the coupling and to provide an easier transition from in-phase to out-of-phase oscillations. We discuss this point in more detail below, but for the moment we set the conductances in the two AMPA couplings different by 10%. In the CPG circuit we set  $g_{\text{AMPA}} = 50$  nS in one synaptic contact and  $g_{\text{AMPA}} = 45$  nS in the other. In the RE-TC system we set  $g_{\text{AMPA}} = 0.2$  nS in one contact and  $g_{\text{AMPA}} = 0.18$  nS in the other.

## A. CPG system

### 1. Precise timing of spike inputs

To indicate the range of circuit responses that result from the incidence of a short sequence of spikes arriving at our CPG circuit, we show in Fig. 4 a series of spike sequences with differing  $T_p$  and also show the result of their action on the circuits. The circuit begins in out-of-phase oscillations. A spike train of  $N_s = 6$  pulses with  $T_p = 150$  ms switches the circuit to in-phase oscillations. Shortly after that a sequence of  $N_s = 15$  pulses with  $T_p = 71$  ms arrives and switches the circuit back to out-of-phase oscillations. While in that out-of-phase state a sequence of  $N_s = 5$  pulses with  $T_p = 180$  ms moves the circuit back to in-phase oscillations. Finally a sequence of  $N_s = 8$  pulses with  $T_p = 125$  ms returns the system to out-of-phase oscillations. Each spike sequence lasts order of 1 s and the switching is typically done by the time two to five spikes have been received.

We note three essential features of these calculations: (i) Inputs of different frequency  $1/T_p$  can switch the behavior from in phase to out of phase and vice versa; (ii) the circuit remains in the state of oscillation selected by the spike train with timing  $T_p$  after the termination of the input; and (iii) the switching can be quite rapid, so the information in the spike train is quickly transferred by the bistable circuit.

The first train of spike inputs with  $T_p = 150$  ms shown in Fig. 4 switches the bursts from out-of-phase behavior to in-phase oscillation. At the onset of the spike train one of the neurons is not affected by the excitatory input because it is in

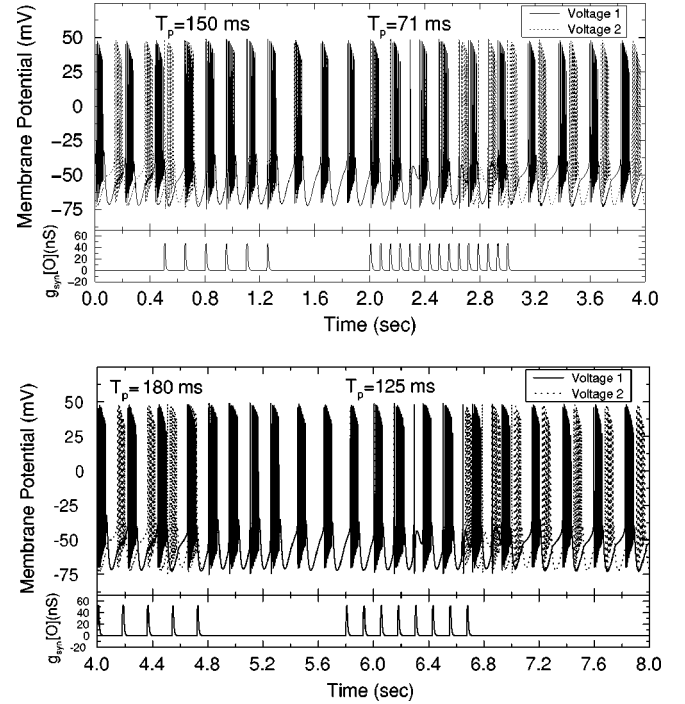


FIG. 4. Time series showing the effect of 1 s of the periodic external forcing in the CPG circuit at several values of  $T_p$ : 150, 71, 180, and 125 ms.

a state where  $I_K(\text{Ca})$  is active or the calcium current is already activated. Therefore, no significant change occurs in this neuron. On the other hand, the second neuron is in a state where only the inward  $I_h$  current is active. So any excitatory input depolarizes the cell to a point where  $I_{\text{Ca}}$  is activated and a burst begins. This allows the second neuron to “catch up” with the other neuron. This phenomenon only happens for a range of  $T_p$ . A second example of this is shown in the bottom panel of Fig. 4 when the neural circuit receives a spike train with  $T_p = 180$  ms.

In-phase bursting can be switched to out-of-phase bursting by stimulating the circuit at different  $T_p$ . This is seen in the parts of Fig. 4 where  $T_p$  is 71 ms and then where it is 125 ms and by introducing nonsymmetric external excitatory input to both neurons. The maximal excitatory conductivity at one of the neurons is 50 nS and 45 nS to the other one. For each  $T_p$  one of the neurons gets activated a little bit earlier than the other one, generating a small delay between them. This delay is sufficient to break the symmetry and transfer the dynamics to out-of-phase oscillations.

In Fig. 5 we look at this switching capability in a different way. We set the electric conductance  $g_{\text{ele}} = 6$  nS. This is in the region of bistable oscillations. We plot the ratio of observed time lag between the oscillations of the CPG neurons to  $T_p$  as a function of  $T_p$ . Figure 5(a) shows this for circuits that are out-of-phase when the spike train arrives and Fig. 5(b) shows this for circuits that are in phase when the spike train arrives. When the system is in phase as the spike train arrives, as seen in Fig. 5(b), we see that for  $62 \text{ ms} \leq T_p \leq 74 \text{ ms}$  the system switches to out-of-phase oscillations. Then, for a broad range of  $T_p$  it remains in phase; for another range of  $T_p$ ,  $105 \text{ ms} \leq T_p \leq 142 \text{ ms}$ , it switches again. Finally, for  $T_p > 142 \text{ ms}$  no switching occurs; the system starts

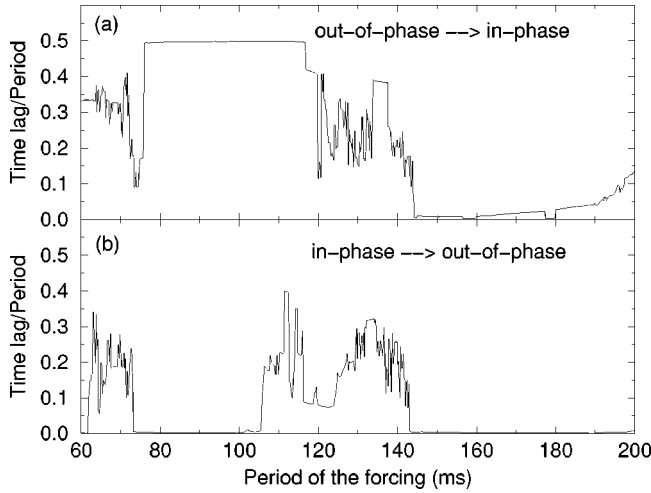


FIG. 5. (Time lag between bursts)/ $T_p$  as a function of  $T_p$ , for the CPG circuit with  $g_{\text{ele}} = 6$  nS and  $g_{\text{GABA}_A} = 20$  nS, when the circuit starts with (a) out-of-phase and (b) in-phase oscillations. In (a) we see that for a wide range of  $T_p$  a circuit starting out of phase stays that way. When  $142 \text{ ms} \leq T_p \leq 180 \text{ ms}$  switching to in-phase (zero time lag) oscillations occurs.

in phase and stays in phase. Similarly, if we begin with out-of-phase oscillations when the spike train arrives, we see in Fig. 5(a) broad regions where the out-of-phase behavior persists and then for  $142 \text{ ms} \leq T_p \leq 180 \text{ ms}$  the spike train switches the oscillations to in-phase behavior. For  $T_p \geq 180 \text{ ms}$  there is some indication of out-of-phase persistence again. In each case reported here the duration of the spike train was about 1 s. This means  $N_s \approx 1 \text{ s}/T_p$  total spikes were received by the circuits.

We have studied the variability as a function of one parameter (the period of the input); however, it is natural to ask what effect the rest of the input parameters have, in particular, the strength of the synaptic input and the duration of the input. We selected four different regions of switching as rel-

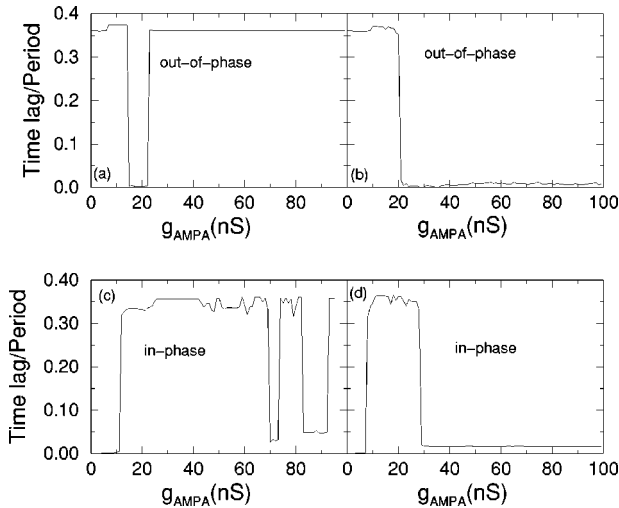


FIG. 6. (Time lag between bursts)/ $T_p$  as a function of the strength of the input for the CPG circuit with  $g_{\text{ele}} = 6$  nS and  $g_{\text{GABA}_A} = 20$  nS, when the circuit starts (a) out of phase with  $T_p = 100$  ms, (b) out of phase with  $T_p = 160$  ms, (c) in phase with  $T_p = 130$  ms, and (d) in phase with  $T_p = 160$  ms.

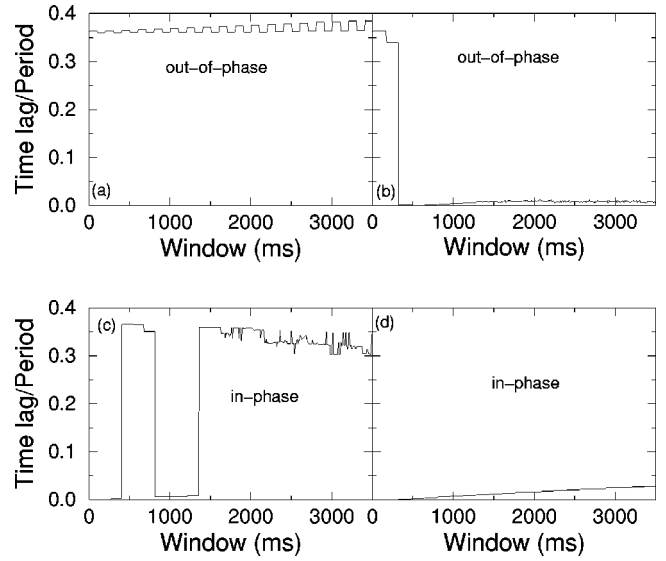


FIG. 7. (Time lag between bursts)/ $T_p$  as a function of the duration of the input for the CPG circuit with  $g_{\text{ele}} = 6$  nS and  $g_{\text{GABA}_A} = 20$  nS, when the circuit starts with (a) out of phase with  $T_p = 100$  ms, (b) out of phase with  $T_p = 160$  ms, (c) in phase with  $T_p = 130$  ms, and (d) in phase with  $T_p = 160$  ms.

evant examples. In Fig. 6 we can see four cases for a given period  $T_p$  of the input. The phase lag versus the strength of the input is plotted. One general observation is displayed: The variability of the time lag does not depend as sensitively on the strength of the input as on the period of the input. Nonetheless, in Fig. 6 we can see a small region where, starting from out-of-phase initial conditions and  $T_p = 100$  ms, in-phase behavior can be achieved. A complementary effect can be observed in Fig. 6(d) where, starting from in-phase initial conditions, out-of-phase behavior is reached. One conclusion is drawn from this figure: If we want the system behavior to change rapidly, the frequency of the input is the best parameter to be chosen. In Fig. 7 we plot the variation of the phase lag as a function of the duration of the input. We can see that from a particular critical value of the input window (stimulus length) there are no changes in the phase lag, which means that if we want to change the state of the system from in-phase to out-of-phase behavior we need a train of 1.5 s, while if we want to transfer the system to out of phase a shorter time of 0.4 s is required.

## 2. Jitter in the spike inputs

To distinguish among these regions of attractor switching, we examined the structural stability of each in the presence of jitter in the timing of the pulses in the incoming spike train. We altered the times at which neurotransmitter release initiates a spike by adding a small random variation to  $t_n$ :

$$t_n = nT_p + T_0 + \Delta t \sigma(t).$$

Again  $\sigma(t)$  is Gaussian white noise with standard deviation unity and  $\Delta t$  is the scale of the allowed timing jitter.

In Fig. 8 we present some results of the effect of timing jitter on the switching ability of our circuits. First, in Fig. 8(a) we start with out-of-phase oscillations and allow a spike train with  $T_p = 160$  ms to arrive at the CPG circuit. If  $\Delta t$

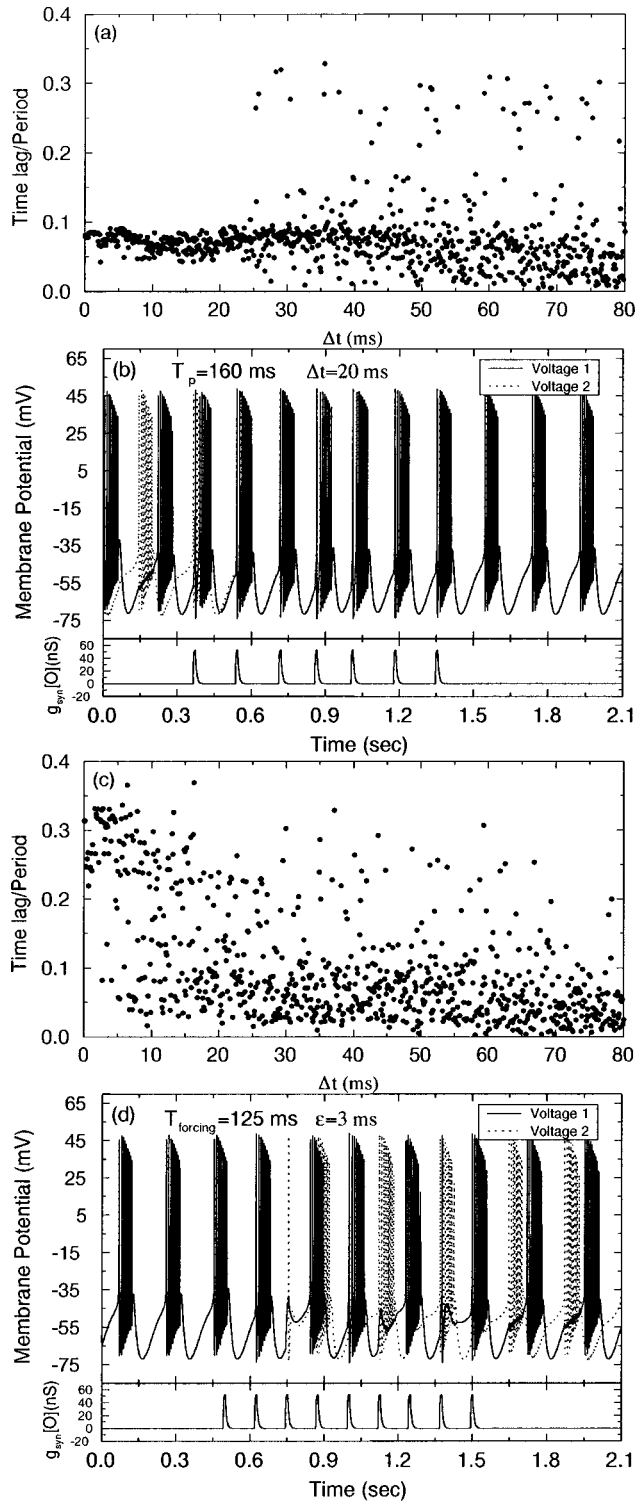


FIG. 8. (a) Ratio of time lag to  $T_p$  as a function of the magnitude  $\Delta t$  of time jitter when we start with out-of-phase initial conditions and the spike train has  $T_p = 160$  ms. When  $\Delta t = 0$ , this situation results in a switch to in-phase (time lag zero) oscillations from out-of-phase motions. (b) Time series for  $T_p = 160$  ms with a jitter of  $\Delta t = 20$  ms. This shows the robustness in switching state despite considerable jitter. (c) Ratio of time lag to period as a function of the magnitude of  $\Delta t$  when we start with in-phase conditions and the spike train has  $T_p = 125$  ms. When  $\Delta t = 0$  this situation results in a switch to out-of-phase oscillations from in-phase oscillations. (d) Time series showing switching with 3-ms jitter and  $T_p = 125$  ms.

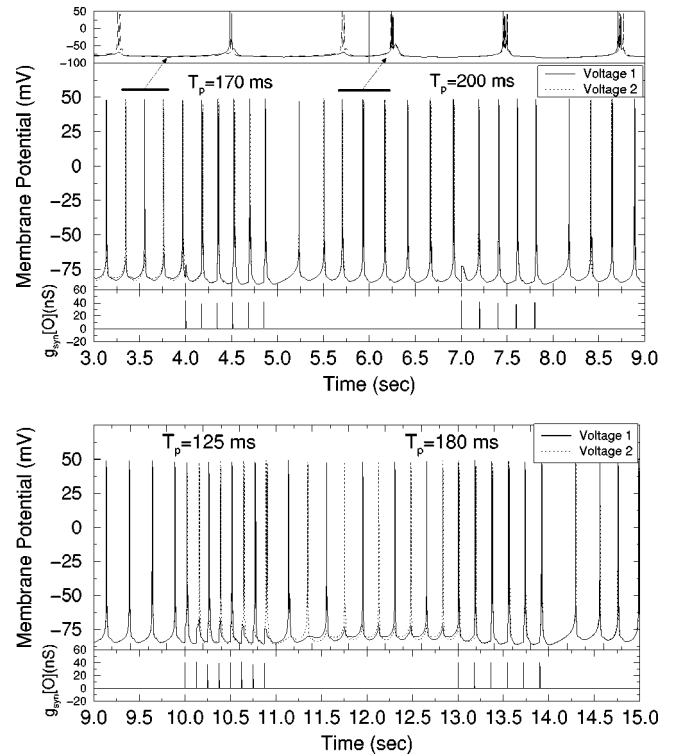


FIG. 9. Time series showing the effect of 1 s of the periodic forcing of the RE-TC circuit at several values of  $T_p$ : 150, 71, 180, and 125 ms. There is an expanded time scale view of the membrane voltage in the RE-TC circuit above the upper panel.

$= 0$ , this would switch the circuit to in-phase behavior as we see from the top panel of Fig. 4. Now we see that this behavior persists for  $0 \leq T_p \leq 25$  ms after which the switching becomes somewhat irregular. A sample of the time series observed with jittery spike trains is seen in Fig. 8(b), where starting from out-of-phase oscillations a spike train with  $T_p = 160$  ms arrives but with  $\Delta t = 20$  ms. The system still switches as it would were  $\Delta t = 0$ .

When we investigate the ability of the system to switch from an initial in-phase state to out-of-phase motion with jitter present, the situation changes. In Fig. 8(c) we show the result of starting in phase and applying a spike train with  $T_p = 125$  ms. If  $\Delta t = 0$ , this would switch the state to out of phase. A sample of the time series observed with jittery spike trains is seen in Fig. 8(d). Now we see that the whole regime is strongly dependent on the magnitude of the jitter. The apparent lack of robustness of in-phase to out-of-phase switching led us to investigate the possibility of delivering the input spike train to the circuits in a nonsymmetric fashion and we take this up below.

## B. Thalamocortical system

Using the same excitatory AMPA couplings now applied to the two TC neurons in the thalamocortical circuit [see Fig. 1(b)] we again investigate the dependence of attractor switching on  $T_p$ . Figure 9 shows the response of the thalamocortical circuit to these external stimuli when the maximal conductance  $g_{GABA_A}$  places the circuit in the region of bistability:  $g_{GABA_A} = 80$  nS. See Fig. 3(c). For  $T_p = 170$  ms and  $T_p = 200$  ms we see that in-phase oscillations

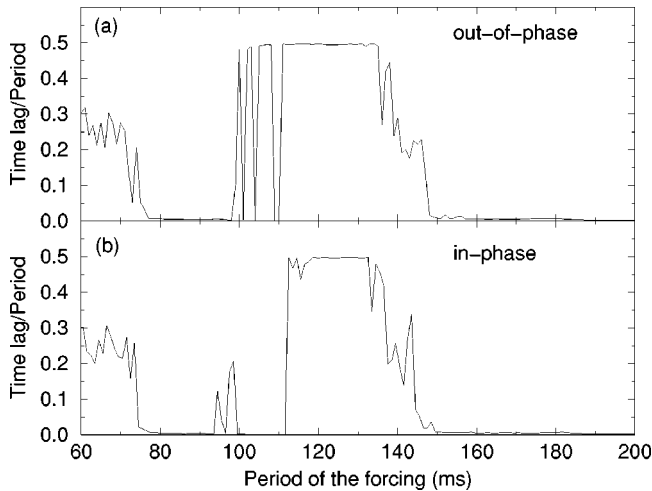


FIG. 10. (Time lag between bursts)/ $T_p$  as a function of  $T_p$  for the RE-TC circuit with  $g_{GABA_A} = 80$  nS. This is in the region of bistability. We show this time lag to  $T_p$  ratio when the circuit starts with (a) out-of-phase oscillations and (b) in-phase oscillations.

remain in phase. When  $T_p$  is changed to 125 ms, the in-phase behavior is switched to out-of-phase oscillations. In turn these out-of-phase motions are switched back to in-phase oscillations when a spike train with  $T_p = 180$  ms arrives. As before, approximately 1 s of input was applied in each case.

Again we present another look at this switching ability by examining what happens first to an out-of-phase oscillation when a spike train of spacing  $T_p$  perturbs it and then ask the same when the spike train perturbs an in-phase oscillation. The upper panel of Fig. 10 summarizes the capability of our excitatory spike trains to switch from initially out-of-phase motions to in-phase motions as a function of  $T_p$ , while the lower panel shows the switching capability from an initially in-phase motion to out-of-phase oscillations as  $T_p$  varies. The time series in Fig. 9 are examples of these switching capabilities.

In qualitative terms the phenomena we see in Fig. 10 can be described by the following. The incoming spike train evokes EPSPs in the thalamic relay cells. The small EPSP that occurs soon after a burst discharge does not affect the TC cell behavior because the inactivation of the low-threshold  $Ca^{2+}$  current  $I_T$  prevents LTS generation. The hyperpolarization of the TC cell deinactivates the  $I_T$  current and the later EPSPs evoke depolarization that results in the LTS. When TC cells oscillate out of phase, the excitatory input changes the behavior of one of the cells and does not influence the behavior of the other. Therefore, the phases of the oscillations are shifted and the TC cells are locked in a regime of in-phase oscillations. Such a mechanism works for specific frequencies only. For higher-frequency stimulation the time delays between EPSPs is not long enough to deinactivate the  $I_T$  current and TC cells show a burst discharge for each second EPSP. This results in their out-of-phase oscillations.

Again we are able to conclude that the three essential features observed in the driven CPG circuit are repeated here: switching, persistence of the switched state after the spike train phases, and rapid switching caused by just a few spikes. The dependence of these effects on the parameters of stimulation was investigated by varying the maximal con-

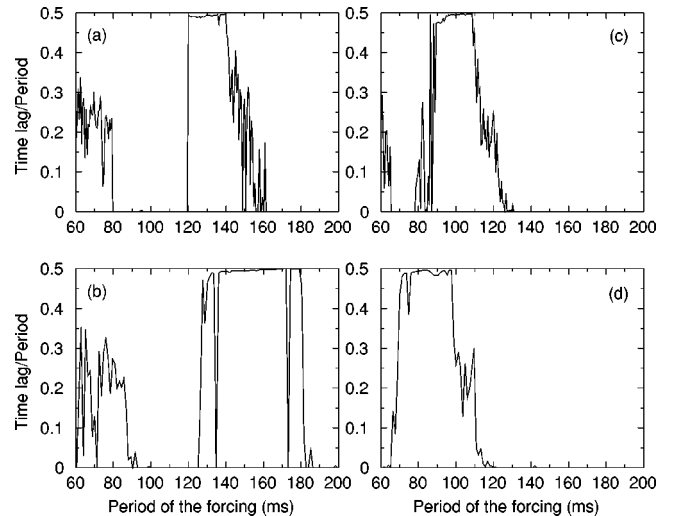


FIG. 11. (Time lag between bursts)/ $T_p$  in the RE-TC circuit as a function of  $T_p$  for four different strengths of the coupling: (a)  $g_{AMPA} = 0.175 \mu S$ , (b)  $g_{AMPA} = 0.15 \mu S$ , (c)  $g_{AMPA} = 0.225 \mu S$ , and (d)  $g_{AMPA} = 0.25 \mu S$ . Changing the maximal conductance of the input AMPA synapses shifts the regions of in-phase and out-of-phase oscillations, but the width of these regions is maintained.

ductance of the input AMPA synapses (amplitude of stimulation). Figure 11 presents the results of this simulation for out-of-phase initial oscillations in the RE-TC circuit. We found that decrease of the maximal conductance [see Figs. 11(a) and 11(b)] shifts the boundaries between in-phase and out-of-phase modes of oscillations to the right (lower frequencies), while increase of the amplitude of stimulation shifts them to the left (higher frequencies). At the same time, the width of the regions where out-of-phase and in-phase oscillations were observed is almost unchanged relative to the amplitude of stimulation (compare Figs. 10 and 11). This result indicates that the strength of the input AMPA synapses is the important parameter controlling stimulus-dependent oscillations in the RE-TC circuit. The change of the maximal conductance for these synapses (e.g., as the concentration of some neuromodulators is changed) may shift the frequency band where the RE-TC circuit is switched from one oscillatory mode to another one. We did not examine the robustness to spike jitter of the detailed results summarized in Fig. 10 for the RE-TC circuits.

#### IV. DISCUSSION

In this paper we have investigated two simple neural circuits coming from two diverse sources. One is a neuron couple connected reciprocally by a gap junction and by inhibitory  $GABA_A$  synapses. It is intended to model a pair of neurons found in the Pyloric CPG of the California spiny lobster, though removed from synaptic connection with the remainder of the CPG neurons. The second is a circuit consisting of coupled pairs of thalamocortical relay and thalamic reticular cells with both inhibitory  $GABA_A$  and  $GABA_B$  couplings as well as AMPA excitatory connections. The common feature of the two circuits is that they have a balancing of influences among their constituent neurons coming from a combination of strong direct couplings, inhibitory couplings, and excitatory couplings. This balance leads in each basic

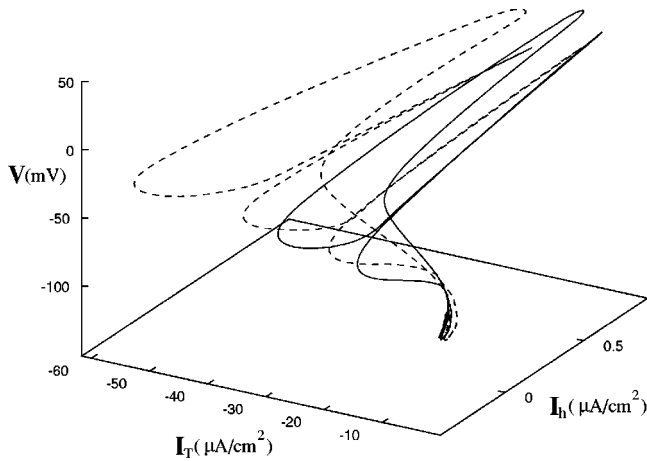


FIG. 12. State space portrait of the two coexisting attractors for the RE-TC system. The solid line is the orbit in  $[V(t), I_T(t), I_h(t)]$  space of the in-phase oscillations. The dotted line is the path taken in the same state space by the out-of-phase oscillations. The closeness of the two attractors leads to the ease with which spike trains with appropriate  $T_p$  can induce transitions between them. The  $GABA_A$  conductances between the RE cells was set at the value 100 nS for each of the state space trajectories in this figure. One can see from Fig. 3 that this places the system in the region of bistability.

circuit to at least one region in their parameter space where bistability and hysteresis occurs. Balanced circuits with more complex connectivity among simpler neural elements have been investigated for their potential role in generating chaotic responses to external input [24].

Bistability occurs when there are two distinct solutions to the conductance based differential equations describing the circuit that coexist over a range of settings of the various parameters in the equations. In this work we explored a range of electrical couplings over which the CPG circuit had two distinct solutions and we investigated a range of  $GABA_A$  coupling over which the RE-TC cells act in the same fashion. In the state space of the systems we see two distinct orbits or phase portraits for the two solution sets. These represent two distinct attractors for the dissipative neural dynamics. Whether after initial transient behavior the circuit ends up on one attractor or another depends on the initial conditions for the solution of the differential equations. In state space each attractor has a set of initial conditions that bring the solution to it and this collection of initial conditions is called its basin of attraction. Figure 12 shows the two attractors for the RE-TC system in the same state space. As one can see, the two attractors are quite close in this space, supporting the fact that transitions between them can be easily induced by the periodic spike trains we introduce.

The model neurons in our circuit were formulated following extensive investigation of conductance based models by earlier workers. Essentially all of the Hodgkin-Huxley dynamics formulated in the Appendix for these circuits has appeared in earlier work. Our starting point in this work was to utilize those formulations and inquire how these circuits from diverse origins but having at least one region of bistability might behave in a common, possibly functional, manner. To explore this we connected each circuit as shown in Fig. 1 to a source of external spike trains with varying inter-

spike interval  $T_p$ . We took spike trains of total length about 1 s over a range  $50 \text{ ms} \leq T_p \leq 250 \text{ ms}$ . Our primary question was whether over broad ranges of  $T_p$  such a short spike train could reset the oscillations of the circuits from one behavior, say in phase, to the other, say out-of-phase, and if so to investigate how robust this resetting would be to noise in the circuit conductances and to error or jitter in the precision of  $T_p$ .

We showed that the short spike train could reset the oscillators over broad values of  $T_p$  in a range of substantial biological interest and, strikingly, we found that the reset, when it occurred, happened in the course of reception of just a few spikes. Long, persistent chains of spikes were not required for the reset. Clearly the spike train acts as a “reset button” for the initial conditions of the coupled neural oscillators pushing the new initial conditions in the other basin of attraction when reset occurs and leaving it in the original basin when reset does not occur. It seems of potential biological importance that reset happens at some  $T_p$  and not others, that reset from in phase to out of phase happens more easily when a time lag or phase difference is present between the two incoming excitatory AMPA inputs, and that there is a distinct robustness to the reset capability against noise in the synaptic conductances and in the precision of  $T_p$ .

Two potential uses may be made of the reset capability of bistable circuits. First, in lobster CPG circuits it is known that neuromodulators can alter the character of neural oscillations in accordance with selected functional behavior [1]. The reset capability of sensory spike trains may also be used to achieve this goal. Second, this reset capability may be a way in which neurons interpret information coming from sensory sources and reformat it for use further along in the animals processing and decision system. If this “learning” function is correct, the mechanism could potentially be useful in short term memory where more complex circuitry would be reset for such a purpose.

The results here also serve as a setting for experimentation [25], especially on the CPG circuit where a couple essentially identical to our model circuit can be identified and isolated in the lobster Pyloric CPG. The results also suggest building a nonlinear circuit model [26] of the neurons and their connections to investigate in a more systematic fashion regions of bi- and multistability and ranges of variation of couplings and interspike intervals than is possible in software explorations.

Finally, as a suggestive model for biomimetic uses, one can view these circuits as sensitive sensors of short pulses of signals with different frequency and phase. Both software and hardware investigations of the range of usable sensitivity of such a sensor would be quite interesting.

#### ACKNOWLEDGMENTS

We thank Rob Elson, Al Selverston, Peter Rowat, and Terry Sejnowski for useful discussions. H.D.I.A. acknowledges the hospitality of Professor A. I. Mees at the University of Western Australia where this manuscript was completed. R.H. and M.I.R. acknowledge support from the U.S. Department of Energy under Grant No. D-FG03-96ER14592 and the NSF under Grant No. IBN-96334405. M.B. was supported by the Sloan Center for Theoretical Neurobiology and

the Howard Hughes Medical Institute. H.D.I.A. was supported in part by the U.S. Department of Energy under Grant No. DE-FG03-90ER14138, in part by the NSF under Grant No. IBN-96334405, and in part by the NSF under Grant No. NCR-9612250. A.K.K. is supported by the Russian Foundation for Basic Research (Project No. 97-02-17526).

## APPENDIX

The general format for conductance models that are the ordinary differential equations of Hodgkin-Huxley type [14] is

$$C_m \frac{dV_i(t)}{dt} = -g_L[V_i(t) - E_L] - \sum_{j=1}^N I_j[V_i(t), t] - \sum_{j=1}^{N_{\text{syn}}} I_j^{\text{syn}}[V_i(t), t] - g_{\text{ele}} \sum_{j \neq i} [V_i(t) - V_j(t)], \quad (\text{A1})$$

where  $V_i(t)$  is the membrane potential of the  $i$ th cell and  $C_m$  is the membrane capacitance.  $g_L$  is the leakage conductance and  $E_L$  its reverse membrane potential.  $g_{\text{ele}}$  is the conductance of the electrical coupling. All intrinsic ionic currents  $I_j[V(t), t]$  have the general form

$$I_j[V(t), t] = g_j m(t)^p h(t)^q [V(t) - E_j], \quad (\text{A2})$$

where  $g_j$  is the maximal conductance.  $m(t)$  represents the activation of the ionic channels and  $h(t)$  the inactivation.  $m(t)$  and  $h(t)$  are dimensionless and lie in the interval  $[0, 1]$ .  $E_j$  is the reversal potential for current  $I_j$ . The time dependence of  $m(t)$  and  $h(t)$  are each assumed to be given as

$$\tau_m(V) \frac{dm(t)}{dt} = m_{\infty}(V) - m(t) \quad (\text{A3})$$

and

$$\tau_h(V) \frac{dh(t)}{dt} = h_{\infty}(V) - h(t), \quad (\text{A4})$$

where  $m_{\infty}(V)$ ,  $h_{\infty}(V)$ ,  $\tau_m(V)$ , and  $\tau_h(V)$  are nonlinear functions of  $V$  extracted from experimental recordings of ionic currents. Unless otherwise stated, the time units for  $\tau_m$  and  $\tau_h$  are milliseconds.  $I_j^{\text{syn}}[V_i(t), t]$  is the current into neuron  $i$  coming from neuron  $j$  through a synaptic connection.

### 1. Stomatogastric circuit

The model stomatogastric neuron is mainly based on [27, 28]. For each cell in the circuit we include a sodium current  $I_{\text{Na}}$ , a persistent sodium current  $I_{p \text{ Na}}$ , a high threshold calcium current  $I_{\text{Ca}}$ , a calcium-dependent potassium current  $I_{\text{K(Ca)}}$ , a delayed-rectifier potassium current  $I_{\text{Kd}}$ , a low threshold  $I_h$  current, and a leakage current  $I_L$ . The voltage time dependence for either neuron in the circuit is given by

$$C_m \frac{dV_i(t)}{dt} = -g_L[V_i(t) - E_L] - I_{\text{Na}}[V_i(t), t] - I_{p \text{ Na}}[V_i(t), t] - I_{\text{Ca}}[V_i(t), t] - I_{\text{Kd}}[V_i(t), t] - I_{\text{K(Ca)}}[V_i(t), t] - I_h[V_i(t), t] - I_{\text{dc}} - g_{\text{ele}} \sum_{j \neq i} [V_i(t) - V_j(t)] - I_{\text{GABA}_A}[V_j(t), t] - I_{\text{ext}}(t). \quad (\text{A5})$$

$I_{\text{GABA}_A}[V_j(t), t]$  is the inhibitory connection reflecting the current seen in neuron  $i$  from the activity of neuron  $j$ ; it is described below.  $I_{\text{ext}}$  is the external perturbation from spike trains injected through AMPA connections and is also described below.  $I_{\text{dc}}$  is a hyperpolarizing dc current injected into each neuron. We took  $I_{\text{dc}} = 0.16$  nA in our computations.  $C_m = 0.33$  nF.

The sodium current has the form

$$I_{\text{Na}}[V(t), t] = g_{\text{Na}} m(t)^3 h(t) [V(t) - E_{\text{Na}}], \quad (\text{A6})$$

with  $g_{\text{Na}} = 70 \mu\text{S}$  and  $E_{\text{Na}} = 50$  mV. In addition, for this current we have

$$\begin{aligned} m_{\infty}(V) &= 1 / \{1 + \exp[(-V - 25.5)/5.29]\}, \\ h_{\infty}(V) &= 1 / \{1 + \exp[(V + 48.9)/5.18]\}, \\ \tau_m(V) &= 1.32 - 1.26 / \{1 + \exp[(-120 - V)/25]\}, \\ \tau_h(V) &= 0.67 \{1 + \exp[(-62.9 - V)/10]\} \\ &\quad \times (1.5 + 1 / \{1 + \exp[(V + 34.9)/3.6]\}). \end{aligned} \quad (\text{A7})$$

The persistent sodium current was taken to be

$$I_{p \text{ Na}}[V(t), t] = g_{p \text{ Na}} m(t)^3 h(t) [V(t) - E_{p \text{ Na}}], \quad (\text{A8})$$

where  $g_{p \text{ Na}} = 3 \mu\text{S}$  and  $E_{p \text{ Na}} = 50$  mV. In addition, for this current we have

$$\begin{aligned} m_{\infty}(V) &= 1 / \{1 + \exp[(-V - 26.8)/8.2]\}, \\ h_{\infty}(V) &= 1 / (1 + \exp(V + 48.5)/4.8W), \\ \tau_m(V) &= 19.8 - 10.7 / \{1 + \exp[(-26.5 - V)/8.6]\}, \\ \tau_h(V) &= 666 - 379 / \{1 + \exp[(-33.6 - V)/11.7]\}. \end{aligned} \quad (\text{A9})$$

We used the calcium current

$$I_{\text{Ca}}[V(t), t] = g_{\text{Ca}} m(t)^3 h(t) [V(t) - E_{\text{Ca}}], \quad (\text{A10})$$

where  $g_{\text{Ca}} = 6 \mu\text{S}$  and  $E_{\text{Ca}} = 120$  mV. In addition, for this current we have

$$\begin{aligned} m_{\infty}(V) &= 1 / \{1 + \exp[(-V - 27.1)/7.18]\}, \\ h_{\infty}(V) &= 1 / \{1 + \exp[(V + 30.1)/5.5]\}, \\ \tau_m(V) &= 30.7 - 21.3 / \{1 + \exp[(-68.1 - V)/20.5]\}, \\ \tau_h(V) &= 105 - 89.8 / \{1 + \exp[(-55 - V)/16.9]\}. \end{aligned} \quad (\text{A11})$$

For the calcium dependent potassium current we took

$$I_{K(\text{Ca})}[V(t),t] = g_{K(\text{Ca})}m(t)^4[V(t) - E_{K(\text{Ca})}], \quad (\text{A12})$$

where  $g_{K(\text{Ca})} = 18.5 \mu\text{S}$  and  $E_{K(\text{Ca})} = 80 \text{ mV}$ . In addition, for this current we have

$$\begin{aligned} m_\infty(V, [\text{Ca}]) &= ([\text{Ca}]/([\text{Ca}] + 3)) \\ &\times \{1 + \exp[(-V - 28.3)/12.6]\}, \\ \tau_m(V) &= 90.3 - 75.1/\{1 + \exp[(-46 - V)/22.7]\}. \end{aligned} \quad (\text{A13})$$

The time dependence of the calcium concentration is taken to satisfy the simplified kinematics

$$\frac{d[\text{Ca}](t)}{dt} = -A I_{\text{Ca}}[V(t),t] - B[\text{Ca}](t) + C, \quad (\text{A14})$$

where  $A = 100 \text{ nM}/(\text{nA ms})$ ,  $B = 5 \text{ ms}^{-1}$ , and the resting calcium concentration is  $C = 50 \text{ nM}/\text{ms}$ . This is a simplification of the intracellular calcium dynamics [29], but for the purposes of this paper, it provides an adequate representation of the influence on calcium on this channel.

The delayed rectifier-potassium current was modeled as

$$I_{Kd}[V(t),t] = g_{Kd}m(t)^4[V(t) - E_{Kd}], \quad (\text{A15})$$

where  $g_{Kd} = 20 \mu\text{S}$  and  $E_{Kd} = 80 \text{ mV}$ . In addition, for this current we have

$$\begin{aligned} m_\infty(V) &= 1/\{1 + \exp[(-V - 12.3)/11.8]\}, \\ \tau_m(V) &= 7.2 - 6.4/\{1 + \exp[(-28.3 - V)/19.2]\}. \end{aligned} \quad (\text{A16})$$

Finally, the low threshold current was taken to be

$$I_h[V(t),t] = g_h m(t)[V(t) - E_h], \quad (\text{A17})$$

where  $g_h = 0.08 \mu\text{S}$  and  $E_h = 20 \text{ mV}$ . In addition, for this current we have

$$\begin{aligned} m_\infty(V) &= 1/\{1 + \exp[(V + 78.3)/6.5]\}, \\ \tau_m(V) &= 272 + 1499/\{1 + \exp[(-42.2 - V)/8.73]\}. \end{aligned} \quad (\text{A18})$$

For the leakage current we set  $g_L = 0.008 \mu\text{S}$  and  $E_L = 65 \text{ mV}$ .

Inhibitory synaptic transmission was modeled using the form of GABA<sub>A</sub> synaptic currents developed for vertebrate neurons. These are described below [30].

## 2. Thalamocortical circuit

The thalamocortical circuit consists of pairs of TC and thalamic RE neurons connected as shown in Fig. 1(b). For each RE and TC cell we included a fast sodium current  $I_{\text{Na}}$ , a fast potassium current  $I_K$  [31], a low-threshold Ca<sup>2+</sup> current  $I_T$  [32,33,20], and a potassium leak current  $I_{KL} = g_{KL}(V - V_{KL})$ . A hyperpolarization-activated cation current  $I_h$  [18,32] and the external AMPA injection  $I_{\text{ext}}(t)$  were also taken into account for the TC cells. The synaptic connections via GABA<sub>A</sub> and GABA<sub>B</sub> inhibition as described below and shown in Fig. 1(b) are also included. The membrane potentials of the neurons are governed by the equations

$$\begin{aligned} C_m \frac{dV_{\text{RE}}(t)}{dt} &= -g_L[V_{\text{RE}}(t) - E_L] - I_{\text{Na}}[V_{\text{RE}}(t),t] \\ &\quad - I_K[V_{\text{RE}}(t),t] - I_{T_{\text{RE}}} - I_{\text{GABA}_A} - I_{\text{AMPA}}, \end{aligned} \quad (\text{A19})$$

$$\begin{aligned} C_m \frac{dV_{\text{TC}}(t)}{dt} &= -g_L[V_{\text{TC}}(t) - E_L] - I_{\text{Na}}[V_{\text{TC}}(t),t] \\ &\quad - I_K[V_{\text{TC}}(t),t] - I_{T_{\text{TC}}} - I_h - I_{\text{GABA}_A} \\ &\quad - I_{\text{GABA}_B} - I_{\text{ext}}(t). \end{aligned}$$

We used  $C_m = 0.143 \text{ nF}$  (area  $1.43 \times 10^{-4} \text{ cm}^2$ ),  $g_L = 7.15 \text{ nS}$ , and  $E_L = -80 \text{ mV}$  for the RE cell [22] and  $C_m = 0.29 \text{ nF}$  (area  $2.9 \times 10^{-4} \text{ cm}^2$ ),  $g_L = 2.9 \text{ nS}$ ,  $E_L = -70 \text{ mV}$ ,  $g_{KL} = 6.4 \text{ nS}$ , and  $E_{KL} = -95 \text{ mV}$  for the TC cells [34].  $I_{\text{ext}}(t)$  is the external AMPA synaptic current discussed in the text. In one AMPA connection we took  $g_{\text{ext}} = 0.2 \text{ nS}$  and in the other  $g_{\text{ext}} = 0.18 \text{ nS}$ .

The sodium current for the RE cells has the form

$$I_{\text{Na}}[V(t),t] = g_{\text{Na}}m(t)^3h(t)[V(t) - E_{\text{Na}}], \quad (\text{A20})$$

with  $g_{\text{Na}} = 14 \mu\text{S}$  and  $E_{\text{Na}} = 50 \text{ mV}$ , while for the TC cells we write

$$I_{\text{Na}}[V(t),t] = g_{\text{Na}}m(t)^3h(t)[V(t) - E_{\text{Na}}], \quad (\text{A21})$$

with the same reversal potential as for RE cells but  $g_{\text{Na}} = 26.1 \mu\text{S}$ . In addition, for both cells we have

$$\begin{aligned} m_\infty(V) &= \alpha_m(V)/[\alpha_m(V) + \beta_m(V)], \\ h_\infty(V) &= \alpha_h(V)/[\alpha_h(V) + \beta_h(V)], \\ \tau_m(V) &= 1/[\alpha_m(V) + \beta_m(V)], \\ \tau_h(V) &= 1/[\alpha_h(V) + \beta_h(V)], \end{aligned} \quad (\text{A22})$$

where

$$\begin{aligned} \alpha_m(V) &= 0.32[13 - v_2(V)](\exp\{[13 - v_2(V)]/4\} - 1)^{-1}, \\ \beta_m(V) &= 0.28[v_2(V) - 40](\exp\{[v_2(V) - 40]/5\} - 1)^{-1}, \\ \alpha_h(V) &= 0.128 \exp\{[17 - v_2(V)]/18\}, \\ \beta_h(V) &= 4/(\exp\{[40 - v_2(V)]/5\} + 1), \\ v_2(V) &= V - (-50). \end{aligned}$$

The potassium current  $I_K$  was modeled as

$$I_K[V(t),t] = g_K m(t)^4[V(t) - E_K], \quad (\text{A23})$$

with  $g_K = 1.43 \mu\text{S}$  and  $E_K = -95 \text{ mV}$  for the RE cells, and

$$I_K[V(t),t] = g_K m(t)^4[V(t) - E_K], \quad (\text{A24})$$

with the same  $E_K$  as for the RE cells and  $g_K = 2.9 \mu\text{S}$  for the TC cells. In addition, for these currents we have

$$m_\infty(V) = \alpha_m(V) / [\alpha_m(V) + \beta_m(V)],$$

$$\tau_m(V) = 1 / [\alpha_m(V) + \beta_m(V)],$$

$$\alpha_m(V) = 0.032 [15 - v_2(V)] (\exp[(15 - v_2(V))/5] - 1)^{-1}, \quad (\text{A25})$$

$$\beta_m(V) = 0.5 \exp\{[10 - v_2(V)]/40\},$$

$$v_2(V) = V - (-50).$$

The  $I_{T_{RE}}$  current for the RE cell was taken to be

$$I_{T_{RE}}[V(t), t] = g_{T_{RE}} m(t)^2 h(t) [V(t) - E_{T_{RE}}], \quad (\text{A26})$$

where  $g_{T_{RE}} = 0.25 \mu\text{S}$  and  $E_{T_{RE}}$  depends on the  $\text{Ca}^{2+}$  concentration inside ( $[\text{Ca}]$ ) and outside ( $[\text{Ca}]_0$ ) the cell. These are defined by the Nerst equation

$$E_{T_{RE}} = \frac{RT}{2F} \ln([\text{Ca}]/[\text{Ca}]_0), \quad (\text{A27})$$

where  $R = 8.31441$ ,  $T = 309.15$ ,  $F = 96489$ , and  $[\text{Ca}]_0 = 2 \text{ mM}$ .

In addition, we have for this current

$$m_\infty(V) = 1 / \{1 + \exp[-(V + 52)/7.4]\},$$

$$\tau_m(V) = (3 + 1 / \{\exp[(V + 27)/10] + \exp[-(V + 102)/15]\}) / \phi_m, \quad (\text{A28})$$

$$h_\infty(V) = 1 / \{1 + \exp[(V + 80)/5]\},$$

$$\tau_h(V) = (85 + 1 / \{\exp[(V + 48)/4] + \exp[-(V + 407)/50]\}) / \phi_h.$$

We have defined the quantities  $\phi_m$  and  $\phi_h$  as

$$\phi_m = \phi_h = 2.5^{(T_C - 24)/10}, \quad (\text{A29})$$

with  $T_C = 36^\circ\text{C}$ .

The  $I_{T_{TC}}$  current is taken to be

$$I_{T_{TC}}[V(t), t] = g_{T_{TC}} m(t)^2 h(t) [V(t) - E_{T_{TC}}], \quad (\text{A30})$$

where  $g_{T_{TC}} = 0.87 \mu\text{S}$  and the reversal potential  $E_{T_{TC}}$  depends on the  $\text{Ca}^{2+}$  concentration in the same way as just noted for the RE cell. In addition, we have for this current

$$m_\infty(V) = 1 / \{1 + \exp[-(V + 59)/6.2]\},$$

$$\tau_m(V) = (1 / \{\exp[-(V + 131.6)/16.7] + \exp[(V + 16.8)/18.2]\} + 0.612) / \phi_m, \quad (\text{A31})$$

$$h_\infty(V) = 1 / \{1 + \exp[(V + 83)/4]\},$$

$$\tau_h(V) = (30.8 + \{211.4 + \exp[(V + 115.2)/5]\}) \times \{1 + \exp[(V + 86)/3.2]\}^{-1} / \phi_h.$$

We have defined the quantities  $\phi_m$  and  $\phi_h$  as

$$\phi_m = 3.55^{(T_C - 24)/10}, \quad \phi_h = 3^{(T_C - 24)/10}, \quad (\text{A32})$$

with  $T_C = 36^\circ\text{C}$ .

Finally, we model the  $I_h$  current for the TC cell as

$$I_h[V(t), t] = g_h m(t) [V(t) - E_h], \quad (\text{A33})$$

where  $g_h = 5.8 \text{ nS}$  and  $E_h = -40 \text{ mV}$ . In addition, we have for this current

$$m_\infty(V) = 1 / \{1 + \exp[(V + 75)/5.5]\},$$

$$\tau_m(V) = (20 + 1000 / \{\exp[(V + 71.5)/14.2] + \exp[-(V + 89)/11.6]\}) / \phi_m, \quad (\text{A34})$$

$$\phi_m = 3^{(T_C - 24)/10},$$

with  $T_C = 36^\circ\text{C}$ . For both RE and TC cells the calcium dynamics is described by a simple model [20]

$$\frac{d[\text{Ca}]}{dt} = -A I_T[V(t), t] - K_T [\text{Ca}] / ([\text{Ca}] + K_d),$$

where  $A = 0.362 \text{ mM/ms } \mu\text{A}$  for the RE cell,  $A = 0.179 \text{ mM/ms } \mu\text{A}$  for the TC cell,  $T = \text{mM/ms}$ , and  $K_d = 0.0001 \text{ mM}$  [35].

### 3. Synaptic couplings

The GABA<sub>A</sub> and AMPA synaptic currents were modeled by a first-order activation scheme (see the review in [36]). The current was given by

$$I_{\text{syn}}[V(t), t] = g_{\text{syn}}[O](t) [V(t) - E_{\text{syn}}],$$

where  $g_{\text{syn}}$  is the maximal conductivity and  $E_{\text{syn}}$  is the reversal potential. For AMPA receptors  $E_{\text{syn}} = 0 \text{ mV}$  and for GABA<sub>A</sub> receptors  $E_{\text{syn}} = -80 \text{ mV}$ .  $[O](t)$  is the fraction of open channels

$$\frac{d[O](t)}{dt} = \alpha \{1 - [O](t)\} [T](t) - \beta [O](t)$$

and  $[T](t)$  is the concentration of transmitter released from time  $t$  to time  $t_{\text{max}}$ ,

$$[T](t) = A \theta(t_{\text{max}} - t) \theta(t),$$

where  $\theta(x)$  is the Heaviside function.

The synaptic parameter values used in the stomatogastric model were chosen as  $A = 1$ ,  $t_{\text{max}} = 9 \text{ ms}$ ,  $\alpha = 0.5 \text{ ms}^{-1}$ , and  $\beta = 0.2 \text{ ms}^{-1}$  for excitatory (AMPA) input synapses and  $A = 1$ ,  $t_{\text{max}} = 3 \text{ ms}$ ,  $\alpha = 0.5 \text{ ms}^{-1}$ , and  $\beta = 0.8 \text{ ms}^{-1}$  for inhibitory (GABA<sub>A</sub>) interconnecting synapses. The strength of the external forcing and the inhibitory coupling are  $g_{\text{AMPA}}$

= 50 nS and  $g_{\text{GABA}_A} = 20$  nS throughout all the numerical integrations. The strength of electrical coupling  $g_{\text{ele}}$  ranges from 0 nS to 20 nS.

The synaptic parameter values used in the thalamocortical model are  $A = 0.5$  and  $t_{\text{max}} = 0.3$  ms and the rate constants were chosen as  $\alpha = 5$  ms and  $\beta = 0.166$  ms for GABA<sub>A</sub> synapses and  $\alpha = 0.94$  ms and  $\beta = 0.18$  ms for AMPA synapses. The strength of the external forcing is  $g_{\text{AMPA}} = 0.2$   $\mu\text{S}$ . The strength of GABA<sub>A</sub> synapses from RE to TC cells is  $g_{\text{GABA}_A} = 0.2$   $\mu\text{S}$  and the coupling between RE cells was varied from 0 and 0.2  $\mu\text{S}$ . The maximal conductance of AMPA synapses is  $g_{\text{AMPA}} = 0.8$   $\mu\text{S}$ .

GABA<sub>B</sub> receptors were described by a more complex activation scheme taking into account the activation of K<sup>+</sup> channels by G proteins [35,22]

$$I_{\text{GABA}_B}[V(t), t] = g_{\text{GABA}_B} \frac{[G]^4}{[G]^4 + K_d} [V(t) - E_k],$$

$$\frac{d[R](t)}{dt} = K_1\{1 - [R](t)\}[T](t) - K_2[R](t), \quad (\text{A35})$$

$$\frac{d[G](t)}{dt} = K_3[R](t) - K_4[G](t),$$

where  $[R](t)$  is the fraction of activated receptors and  $[G](t)$  is the concentration of G proteins. In these equations we chose  $K_1 = 0.52$ ,  $K_2 = 0.0013$ ,  $K_3 = 0.098$ ,  $K_4 = 0.033$ , and  $K_d = 100$ .  $g_{\text{GABA}_B} = 0.05$   $\mu\text{S}$ .

- 
- [1] A. I. Selverston and M. Moulins, *The Crustacean Stomatogastric System* (Springer-Verlag, Berlin, 1987).
- [2] M. Steriade, D. A. McCormick, and T. J. Sejnowski, *Science* **262**, 679 (1993).
- [3] P. S. Katz, P. A. Getting, and W. N. Frost, *Nature (London)* **367**, 729 (1994).
- [4] S. L. Hooper, *Neural Representation of Temporal Patterns* (Plenum, New York, 1995), pp. 107–128.
- [5] J. E. Lisman, *Trends Neurosci.* **20**, 38 (1997).
- [6] M. Steriade and R. Llinás, *Physiol. Rev.* **68**, 649 (1988).
- [7] H. D. I. Abarbanel, R. Huerta, M. I. Rabinovich, N. F. Rulkov, P. Rowat, and A. I. Selverston, *Neural Comput.* **8**, 1567 (1996).
- [8] S. K. Han, C. Kurrer, and Y. Kuramoto, *Phys. Rev. Lett.* **75**, 3190 (1995).
- [9] A. Sherman and J. Rinzel, *Proc. Natl. Acad. Sci. USA* **89**, 2471 (1992).
- [10] C. van Vreeswijk, L. F. Abbott, and G. B. Ermentrout, *J. Comput. Neurosci.* **1**, 313 (1994).
- [11] R. Huerta, M. I. Rabinovich, H. D. I. Abarbanel, and M. Bazhenov, *Phys. Rev. E* **55**, R2108 (1997).
- [12] A. Sherman, *Bull. Math. Biol.* **56**, 811 (1994).
- [13] H. D. I. Abarbanel, *Analysis of Observed Chaotic Data* (Springer-Verlag, New York, 1996).
- [14] A. L. Hodgkin and A. F. Huxley, *J. Physiol. (London)* **117**, 500 (1952).
- [15] W. H. Enright, D. J. Higham, B. Owren, and P. W. Sharp (unpublished), available at <http://www.cs.toronto.edu/>.
- [16] S. D. Cohen and A. C. Hindmarsh, *CVODE User Guide*, Lawrence Livermore National Laboratory Report No. UCRL-MA-118618, 1994 (available at <http://netlib2.cs.utk.edu/cgi-bin/>).
- [17] G. Engeln-Mullges and F. Uhlig, *Numerical Algorithms with C* (Springer, Berlin, 1996), pp. 449–450.
- [18] D. A. McCormick and H. C. Pape, *J. Physiol. (London)* **431**, 291 (1990).
- [19] M. Steriade, R. Curró Dossi, and A. Nuñez, *J. Neurosci.* **11**, 3200 (1991).
- [20] A. Destexhe, D. Contreras, T. Sejnowski, and M. Steriade, *J. Neurophysiol.* **72**, 803 (1994).
- [21] D. Golomb, X.-J. Wang, and J. Rinzel, *J. Neurophysiol.* **72**, 1109 (1994).
- [22] A. Destexhe, T. Bal, D. A. McCormick, and T. J. Sejnowski, *J. Neurophysiol.* **76**, 2049 (1996).
- [23] D. Golomb, X.-J. Wang, and J. Rinzel, *J. Neurophysiol.* **75**, 750 (1996).
- [24] C. van Vreeswijk and H. Sompolinsky, *Science* **274**, 1724 (1996).
- [25] M. Maher, R. Elson, and A. I. Selverston (private communication).
- [26] N. F. Rulkov and A. Volkovskii (private communication).
- [27] G. Turrigiano, G. LeMasson, and E. Marder, *J. Neurosci.* **15**, 3640 (1995).
- [28] F. Buchholtz, J. Golowasch, I. R. Epstein, and E. Marder, *J. Neurophysiol.* **67**, 332 (1992).
- [29] Y.-X. Li, S. S. Stojilkovic, J. Keizer, and J. Rinzel, *Biophys. J.* **72**, 1080 (1997).
- [30] The programs for integrating this stomatogastric model can be requested from [huerta@jario.ucsd.edu](mailto:huerta@jario.ucsd.edu).
- [31] R. D. Traub and R. Miles, *Neuronal Networks of the Hippocampus* (Cambridge University Press, Cambridge, 1991).
- [32] J. R. Huguenard and D. A. Prince, *J. Neurosci.* **12**, 3804 (1992).
- [33] J. R. Huguenard and D. A. McCormick, *J. Neurophysiol.* **68**, 1373 (1992).
- [34] D. A. McCormick and J. R. Huguenard, *J. Neurophysiol.* **68**, 1384 (1992).
- [35] The programs for integrating this RE-TC model are available on request by e-mail to [bazhenov@salk.edu](mailto:bazhenov@salk.edu).
- [36] A. Destexhe, Z. F. Mainen, and T. J. Sejnowski, *J. Comput. Neurosci.* **1**, 195 (1994).